

Improving Metric Dimensionality Reduction with Distributed Topology

Alexander Wagner*

Department of Mathematics,
Duke University
Durham, USA
alexander.wagner@duke.edu

Elchanan Solomon*

Department of Mathematics,
Duke University
Durham, USA
yitzchak.solomon@duke.edu

Paul Bendich

Department of Mathematics, Duke University
Geometric Data Analytics
Durham, USA
paul.bendich@duke.edu

Abstract—We propose a novel approach to dimensionality reduction combining techniques of metric geometry and distributed persistent homology, in the form of a gradient-descent based method called **DIPOLE**. **DIPOLE** is a dimensionality-reduction post-processing step that corrects an initial embedding by minimizing a loss functional with both a local, metric term and a global, topological term. By fixing an initial embedding method (we use **Isomap**), **DIPOLE** can also be viewed as a full dimensionality-reduction pipeline. This framework is based on the strong theoretical and computational properties of distributed persistent homology and comes with the guarantee of almost sure convergence. We observe that **DIPOLE** outperforms popular methods like **UMAP**, **t-SNE**, and **Isomap** on a number of popular datasets, both visually and in terms of precise quantitative metrics.

I. INTRODUCTION

The goal of dimensionality reduction is to replace a high-dimensional data set with a low-dimensional proxy that has a similar shape. The terms *similar* and *shape* are not strictly defined, and a wealth of dimensionality reduction methods exists to accommodate the manifold ways of formulating the problem. Classical methods like PCA and MDS (Kruskal, 1964) are concerned with globally preserving variance or pairwise distances in a data set. These methods are of great utility in machine learning as a whole, but produce poor results on data sets that are not metrically low-dimensional. This has prompted the introduction of methods that emphasize preserving local structure over global structure, such as locally linear embeddings (Roweis and Saul, 2000), Laplacian eigenmaps (Belkin and Niyogi, 2003) and diffusion maps (Coifman and Lafon, 2006), **Isomap** (Tenenbaum et al., 2000), and more recently, **t-SNE** (van der Maaten and Hinton, 2008) and **UMAP** (McInnes et al., 2018). Each method has its own way of encoding a high-dimensional data set, e.g. via a connectivity graph, using random walks, as a probability

distribution, etc., and its own scheme for preserving the metric, spectral, or distributional properties of that data structure in a low-dimensional embedding.

To our mind, there are two important limitations of the above-mentioned dimensionality reduction methods. Firstly, there are many cases in which some or all of the global geometry of a data set can be preserved by a low-dimensional embedding, but these local methods are not guaranteed to find such an embedding. Secondly, there are important global features of shapes that are not metric but topological, and as none of these local methods compute topological invariants, they cannot guarantee preservation of topological structure.

Our goal is to show that distributed persistence, as defined in Solomon et al. (2021), can be used to augment local metric methods and address both of the above challenges simultaneously. To be precise, we will show that:

- 1) Distributed persistence provides a scalable, parallelizable framework for incorporating topological losses into dimensionality reduction methods.
- 2) Distributed persistence can provide strong guarantees for preservation of global structure, when feasible.
- 3) Gradient descent with distributed persistence provably converges.
- 4) Incorporating persistence into dimensionality reduction provides improved embeddings on a number of standard data sets.

We call our method **DIPOLE**: Distributed Persistence-Optimized Local Embeddings. The word *dipole* comes from the Greek $\delta\acute{\iota}\zeta\ \pi\acute{o}\lambda\omicron\varsigma$ meaning *doubled axes*. In our framework, the two axes are local geometry and global topology, which play both complementary and competitive roles in obtaining optimal embeddings.

A. Why persistent homology?

Unlike more ad hoc methods for measuring the shape of data, persistent homology is rooted in algebraic topology and enjoys strong theoretical foundations. Persistent homology captures topology on many scales at once, and so is not limited by the need to fix a scale parameter. The output of persistent homology is differentiable almost everywhere as a function of the input data (Gameiro et al., 2016) and (Poulenard et al., 2018), allowing for its incorporation in gradient

The first author was partially supported by the National Science Foundation under the grant “HDR TRIPODS: Innovations in Data Science: Integrating Stochastic Modeling, Data Representations, and Algorithms”, NSFCCF-1934964. The second and third authors were partially supported by the Air Force Office of Scientific Research under the grant “Geometry and Topology for Data Analysis and Fusion”, AFOSR FA9550-18-1-0266. The MR brain images from healthy volunteers used in this paper were collected and made available by the CASILab at The University of North Carolina at Chapel Hill and were distributed by the MIDAS Data Server at Kitware, Inc.

* Equal contribution

descent optimization schemes (Carriere et al., 2021). Persistent homological features (barcodes, persistence diagrams, Betti curves, Euler curves, etc.) can be directly compared with one another (Cohen-Steiner et al., 2007), subjected to statistical analysis (Mileyko et al., 2011) and (Fasy et al., 2014), and transformed into feature vectors (Bubenik, 2015) and (Adams et al., 2017).

B. Why distributed persistence?

Persistence calculations scale poorly in the size of data sets (Otter et al., 2017), are not robust to outliers (Buchet et al., 2014), and leave out a lot of information about the shape of data (Curry, 2018). Distributed persistence overcomes these limitations through random subset sampling: instead of computing the persistence diagram of the full data set, one computes the persistence diagrams of many small subsets. This has the effect of producing a much faster and more robust invariant. Moreover, distributed persistence is considerably more informative than full persistence, as spaces with similar distributed persistences are necessarily quasi-isometric.

It is natural to ask why, if distributed persistence invariants contain global metric data, we do not simply use global metric data directly. There are three main reasons:

- When global geometry-preserving embeddings are impossible (which is generally the case), preserving distributed persistence is not equivalent to preserving quasi-isometry type. The latter is futile whereas the former amounts to fixing the topology, which may indeed be possible.
- When there are embeddings that preserve global geometry within reasonable error, there may generally be many such embeddings, some of which are more topologically faithful than others. By working with distributed persistence, we can obtain a quasi-isometry that also has nice topological properties.
- It is sometimes possible to find an embedding that is a quasi-isometry on a subset of a space. An embedding method based on fixing topology may be able to capture the global geometry on this subset and the topological type of its complement.

We see DIPOLE as a dimensionality-reduction post-processing step. Starting with an initialization embedding, obtained by methods such as t-SNE, UMAP, or Isomap, DIPOLE corrects the topology using distributed persistence. The use cases of focus in this paper are data sets which exhibit low intrinsic dimension and marked topological and metric structures. Examples include manifolds, algebraic varieties, configuration spaces, graphs, and more general embedded simplicial complexes. For such spaces, it is often possible to find low-dimensional embeddings that preserve geometry on small scales and maintain large-scale topology.

II. PRIOR WORK

There have been other lines of research aimed at incorporating topology into dimensionality reduction. Doraiswamy et al. (2020) aim to maintain global degree-zero persistence

by preserving the minimal spanning tree of the original data embedding in the projection. Shieh et al. (2011) study embeddings preserving the single-linkage dendrogram of a data set. Yan et al. (2018) consider an extension of landmark Isomap (De Silva and Tenenbaum, 2004) that uses homology to pick optimal landmarks. Moor et al. (2020) add a topological loss term to improve latent space representations of autoencoders. These approaches differ from ours in two ways: only Moor et al. (2020) optimize on topological invariants directly, and none of the prior methods use distributed persistence.

A. Outline of Paper

Section III defines distributed persistence and states theorems from Solomon et al. (2021) highlighting its inverse properties. Section IV explains the dimensionality reduction pipeline used in DIPOLE. Section V provides a proof of almost sure convergence for the gradient descent scheme underlying DIPOLE. Section VI compares DIPOLE to other popular methods on a number of challenging data sets. Finally, VII summarizes the results of the paper and outlines directions for future research.

III. DISTRIBUTED PERSISTENCE

We provide a summary of the results from Solomon et al. (2021), and indicate how they relate to the task of dimensionality reduction. Let λ be an invariant of finite metric spaces. Let X be an abstract indexing set, and $\psi : X \rightarrow Z$ an embedding into a metric space Z . For $k \in \mathbb{N}$, we define the distributed invariant λ_k that maps the labeled point cloud (X, ψ) to the labeled set of invariants $\{\lambda(\phi(S)) \mid S \subseteq X, |S| = k\}$ for $k > 0$, and \emptyset otherwise. Put another way, $\lambda_k(X, \psi)$ records the values of λ on subsets of $\psi(X)$ of a fixed size, together with abstract labels identifying which invariant corresponds to which subset. In what follows, we will omit the embedding map ψ and refer to X as a metric space directly, unless it becomes necessary to distinguish between X as an indexing set and X as a metric space.

When the invariant λ is expensive to compute, as is the case for persistent homology, λ_k provides a scalable, parallelizable alternative. λ_k enjoys all of the stability properties of λ (cf. Cohen-Steiner et al. (2007)), since it is computed in the same way, but is generally more robust to outliers, since λ_k is unchanged on those subsets of X that do not contain an outlier. The main result of Solomon et al. (2021) is that the topology of many small subsets can be used to recover the isometry type of X up to a multiplicative error term that is generally quadratic (but sometimes linear) in the size of the subsets taken:

Theorem 1. *Let λ^m be the invariant that associates to a point cloud the Rips persistence of its m -skeleton, and take $k > m > 0$. Let $\phi : X \rightarrow Y$ be a surjection¹ such that for all $S \subseteq X$ with $|S| \in \{k, k-1, \dots, k-m-1\}$,*

¹The original version of this result assumes ϕ is a bijection, but relaxing it to a surjection has no impact on the proof.

$d_B(\lambda^m(S), \lambda^m(\phi(S))) \leq \epsilon^2$ Then ϕ is a $112k^2\epsilon$ quasi-isometry, i.e. $\forall x_1, x_2 \in X$,

$$|d_X(x_1, x_2) - d_Y(\phi(x), \phi(y))| \leq 112k^2\epsilon.$$

Note that when $\epsilon = 0$, ϕ must be an isometry, showing that the invariant sending X to the topology of many small subsets is injective. The above theorem extends injectivity by showing that the inverse is Lipschitz from the Bottleneck distance d_B to the quasi-isometry metric. This result can be improved to give linear dependence on the subset size k , provided ϕ is known to restrict to a quasi-isometry on a small subset of X :

Theorem 2. Let $k > m = 1$. Let $\phi : X \rightarrow Y$ be a surjection such that for all $S \subseteq X$ with $|S| \in \{k, k-1\}$, $W_1(\lambda^1(S), \lambda^1(\phi(S))) \leq \epsilon_1$.³ Suppose further that there is a subset $X' \subset X$ of size $(k-1)$ with

$$\sum_{(x_i, x_j) \in X' \times X'} |d_X(x_i, x_j) - d_Y(\phi(x_i), \phi(x_j))| \leq \epsilon_2.$$

Then ϕ is a $56(k+1)\epsilon_1 + 28\epsilon_2$ quasi-isometry.

One can paraphrase this result as follows: assuming that ϕ is already known to preserve distances on a small subset $X' \subset X$, its maintaining of small-scale topology gives a linear bound on global metric distortion. This motivates a pipeline in which we initialize our embedding ϕ to preserve local distances, and add an extra term to our topological loss (the *local metric regularizer*) that protects this local correctness, so that we do not violate the hypothesis of Theorem 2 over the course of the optimization.

Remark 3. In fact, one does not need to show that ϕ preserves topology on *all* small subsets of cardinality $|S| \in \{k, \dots, k-m-1\}$ to ensure a quasi-isometry, as a relatively small number of subsets suffices. Details and extensions of these results can be found in Solomon et al. (2021).

IV. DIMENSIONALITY REDUCTION

Having provided an overview of the definition and advantages of distributed persistence, we now go into the details of our pipeline. Let (X, d_X) be a finite metric space, not necessarily embedded in Euclidean space. For a given $n \in \mathbb{N}$, our goal is to find a function $f : X \rightarrow \mathbb{R}^n$ that preserves important metric and topological features of X . To that end, we want to define a loss on embedding functions that is sufficiently differentiable to allow for gradient descent optimization. We define a loss with both a local metric term and a global topological term.

We begin with the local metric term. Let $P \subseteq X \times X$ be a subset of pairs of points in X . Intuitively, the pairs of points in P should be thought of as being close to one another. One

²The output of λ^m is a collection of persistence diagrams, one for each homological degree up to m . The bottleneck distance here is the maximum of the bottleneck distances across all degrees.

³The W_1 distance here is the sum of the W_1 distances for the zero and first degree persistent homology.

way of producing such a set P is to pick a radius parameter $\delta > 0$ and define:

$$P = \{(x_i, x_j) \in X \times X \mid d_X(x_i, x_j) \leq \delta\}.$$

Another possibility is to pick an integer ℓ and define P to consist of those pairs (x_i, x_j) where x_i is one of x_j 's ℓ -nearest neighbors, or the reverse.

With our set P in hand, we can define the *local metric regularizer functional*, LMR_P , defined as follows:

$$LMR_P(f) = \sum_{(x_1, x_2) \in P} (d_X(x_1, x_2) - \|f(x_1) - f(x_2)\|)^2.$$

For the global topological term of our loss, we turn to distributed persistence, and define the functional $DP_k^m(f)$ as follows:

$$DP_k^m(f) = \frac{1}{\binom{|X|}{k}} \sum_{\substack{S \subset X \\ |S|=k}} W_p^p(\lambda^m(S), \lambda^m(f(S))).$$

where W_p is the p -Wasserstein distance between diagrams. Since we are working with persistent homology in multiple degrees, we sum up the W_p^p -distance among all degrees. Viewing the embedding f as a matrix of shape $n \times |X|$, this functional is differentiable almost everywhere with respect to the entries of the matrix, so that gradient descent optimization can be applied. Due to the huge number of terms in the sum, and in light of Remark 3, we opt for stochastic gradient descent, randomly sampling a small batch of subsets of size k whose persistence are computed. Thus our pipeline is the following: we initialize our embedding f_0 and then apply some form of gradient descent to the functional $\alpha LMR_P + DP_k^m$.

V. CONVERGENCE

Our aim in this section is to prove that gradient descent on the functional $\Phi = \alpha LMR_P + DP_k^m$ converges almost surely. Assuming our point cloud consists of s points in \mathbb{R}^d , we can encode it as an element of \mathbb{R}^{ds} . We write $X_0 \in \mathbb{R}^{ds}$ for the initial point cloud, and $X_n \in \mathbb{R}^{ds}$ for the point cloud after n stochastic gradient descent steps. Our proof relies on the techniques developed in Davis et al. (2020), which we now recall.

Let $\Phi : \mathbb{R}^{ds} \rightarrow \mathbb{R}$ be locally Lipschitz, and let $\partial\Phi(x)$ denote the *Clarke subdifferential* of Φ at a point $X \in \mathbb{R}^{ds}$. Starting at an initial point $X_0 \in \mathbb{R}^{ds}$, the *stochastic subgradient method* consists of the following iteration: $X_{n+1} = X_n - \alpha_n(y_n + \xi_n)$, where α_n is a step size, $y_n \in \partial\Phi(X_n)$ is an element of the Clarke subdifferential, and ξ_n is a sequence of random variables modeling noise. It is shown in Davis et al. (2020) (Corollary 5.9) that the following four conditions (the first three are called *Assumption C*) guarantee almost sure convergence:

- 1) The sequence α_n is nonnegative, square summable ($\sum_n \alpha_n^2 < \infty$) but not summable ($\sum_n \alpha_n = \infty$).
- 2) The iterates are a.s. bounded, $\sup \|X_n\| < \infty$.
- 3) The sequence $\{\xi_n\}$ is a martingale difference sequence, i.e. almost surely we have $\mathbb{E}[\xi_n] = 0$ and $\mathbb{E}[\|\xi_n\|^2] < \infty$.

$p(x_n)$, where p is some function bounded on bounded sets.

4) f is C^d -stratifiable.

For definitions of technical terms like Clarke subdifferential or stratifiability, cf. Davis et al. (2020).

A. Our Setting

Before proceeding to the proof, we explain how DIPOLE fits into the framework of Davis et al. (2020).

We perform gradient descent by randomly picking some number of subsets of size k , and using the gradients on those subsets to take a descent step. Since $\partial\Phi$ takes into account *all* subsets, we need some way of subtracting off the gradients for all those subsets not sampled. This is accomplished by a careful definition of ξ_n . To begin, we randomly pick b subsets S_1, \dots, S_b of size k , consider the sum $\hat{\Phi} = \frac{1}{b} \sum_{i=1}^b W_p^p(\lambda^m(S_i), \lambda^m(\phi(S_i))) + \alpha LMR_P$, and take a random element $v_n \in \partial\hat{\Phi}(x_n)$. It is this element v_n that we use in DIPOLE. We therefore set $\xi_n = y_n - v_n$, so that $y_n - \xi_n = v_n$. In other words, we define ξ_n to cancel out the effect of all unsampled subsets, leaving only the sampled gradient.

We now point out two important features of Φ . Firstly, Φ is the sum of a smooth function (the local metric regularizer) and persistence functionals (which are locally Lipschitz), so Φ itself is locally Lipschitz, and the results of Davis et al. (2020) apply. Secondly, since both the local metric regularizer and persistence functionals are translation invariant, Φ is also translation invariant. We use the translation invariance to replace the original sequence X_n with a mean-centered sequence \bar{X}_n that is easier to control.

Definition 4. Let $X \in \mathbb{R}^{ds}$ represent a point cloud of s points in \mathbb{R}^d . Define $\bar{X} \in \mathbb{R}^{ds}$ to be the result of mean-centering the point cloud. Identifying \mathbf{R}^{ds} with the vector space of matrices $M_{d \times s}$, we have

$$\bar{X} = X(I - \frac{1}{s}J)$$

where I is the $s \times s$ identity matrix, and J is an $s \times s$ matrix containing only 1s.

The following theorem requires that (X, P) be a connected subgraph of X . This is analogous to the assumption inherent in Isomap that the shortest path metric on the k -nearest-neighbors subgraph of a point cloud has no infinite values.

Theorem 5. *Suppose $\alpha > 0$ and (X, P) is a connected subgraph of X . Then the mean-centered sequence \bar{X}_n converges to a critical point for Φ , and $\Phi(X_n) = \Phi(\bar{X}_n)$ converges.*

B. The Proof

Before working through the four conditions guaranteeing a.s. convergence in Davis et al. (2020), we justify replacing X_n with \bar{X}_n . In order to apply the convergence results of Davis et al. (2020) to \bar{X}_n , we need to show that \bar{X}_n also arises from a stochastic gradient descent scheme. The subtlety here is the following: \bar{X}_n and \bar{X}_{n+1} are obtained by mean-centering X_n and X_{n+1} , respectively, but it is not necessarily

the case that a gradient descent step at \bar{X}_n produces \bar{X}_{n+1} , i.e. that mean-centering commutes with taking gradients. A failure of commutativity would mean that $\{\bar{X}_n\}$ is not the product of an actual stochastic gradient descent scheme, and hence is not eligible for the application of prior convergence results.

To show commutativity, we observe that \bar{X} sits inside the subvariety \mathcal{X} of $M_{d \times s}$ consisting of mean-centered point clouds. \mathcal{X} can also be characterized as the range of the projection $T(X) = X(I - \frac{1}{s}J)$. As $I - \frac{1}{s}J$ is symmetric, T is an orthogonal projection. Given a point $X \in \mathcal{X}$ and a gradient $\epsilon \in \partial\Phi(X)$ in the full tangent space to $M_{d \times s}$, we then know that the orthogonal projection of ϵ to the tangent space at \mathcal{X} is $T(\epsilon)$. Thus, if $X_{n+1} = X_n + \alpha_n \epsilon$,

$$\begin{aligned} \bar{X}_{n+1} &= T(X_{n+1}) \\ &= T(X_n + \alpha_n \epsilon) \\ &= T(X_n) + T(\alpha_n \epsilon) \\ &= \bar{X}_n + \alpha_n T(\epsilon). \end{aligned}$$

This demonstrates that \bar{X}_{n+1} is obtained from \bar{X}_n by taking a descent step in \mathcal{X} , and so mean-centering commutes with gradient descent. Lastly, since \mathcal{X} is isometric to $\mathbb{R}^{(d-1) \times s}$, the results of Davis et al. (2020), framed in Euclidean space, apply equally well to \mathcal{X} . The major advantage of working with $\{\bar{X}_n\}$ is the following lemma.

Lemma 6. *The sequence $\{\bar{X}_n\}$ is a.s. bounded.*

Proof. We first show that the diameter of the mean-centered point clouds $\{\bar{X}_n\}$ is a.s. bounded. Note that the diameter of a point cloud can be bounded without the point cloud being bounded; for a simple example, consider a single point (diameter zero) wandering off to infinity.

Suppose that the diameter of our point cloud is not bounded. Since (X, P) is connected, some edge in P is growing without bound, and hence the local metric regularizer is growing without bound. Clearly, the gradient term coming from the local metric regularizer cannot cause this to happen, so the only possibility is that this is an effect of the topological loss. However, a topological gradient on a very long edge corresponds to a point in a persistence diagram with very large birth or death time, and since the target distributed persistence is bounded, a Wasserstein matching will either push such a point closer to a bounded region in the upper-half quadrant, or else its projection on to the diagonal, and in either case it will not grow without bound.

To conclude that the point clouds $\{\bar{X}_n\}$ are bounded, suppose again the converse. This means that some coordinate of some point is growing without bound. In order for the point cloud to remain mean-centered, the same coordinate of another point must also be growing without bound, and of the opposite sign. This forces the diameter of the point cloud to grow without bound, which we have already shown is impossible. Thus, the mean-centered sequence is a.s. bounded. \square

We now work through the four conditions guaranteeing a.s. convergence, noting that mean-centering has no effect on local quantities like the errors ξ_n .

(1) The condition on the learning rate α_n is easily satisfied by setting $\alpha_n = \frac{1}{n}$, as well as any other of a number of annealing schemes.

(2) This was shown in the Lemma above.

(3) To see that $\mathbb{E}[\xi_n] = 0$, observe that any subset of X is equally likely to be chosen when generating ξ_n , so the expected value of v_n is an element of the full Clarke subdifferential $\partial\Phi(X_n)$. Since X_n is generically non-critical, $\partial\Phi(X_n)$ consists of a single vector, so that $\mathbb{E}[v_n] = y_n$ and $\mathbb{E}[\xi_n] = 0$. To see that the variance of ξ_n is bounded, note that Φ is the sum of finitely many functions, each of which has subgradient bounded when the point cloud has bounded diameter. Thus the subgradients of Φ and $\hat{\Phi}$ are likewise bounded on bounded sets, and so the same is true for $\|\xi_n\|^2$, even without having to take expectations.

(4) The last condition, that Φ is C^d -stratifiable, follows from persistence functionals being locally linear (details can be found in Carriere et al. (2021)).

VI. EXPERIMENTS

The exact formula for the loss function used in experiments is given in Equation (1). Like other dimensionality reduction pipelines, DIPOLE depends on the choice of hyperparameters. Our default choices are:

- The default initialization embedding is produced via Isomap. Isomap is fast and non-stochastic, and is designed to preserve local distances, a criterion in line with Theorem 2.
- When the input data is a point cloud in Euclidean space, it is transformed into a distance matrix by taking the geodesic distance on the m_1 -nearest-neighbor graph, for $2 \leq m_1 \leq 10$.
- We set the learning rate in $\{0.1, 1\}$, and the tradeoff parameter $\alpha \in \{0.01, 0.1\}$.
- The set P is chosen to consist of the m_2 -nearest neighbors of points in X . We typically take $2 \leq m_2 \leq 5$.
- We fix $p = 2$ in the Wasserstein distance.
- We run 2500 descent steps, using the annealing factor $\frac{1000}{1000+\text{step}}$.

The target dimension and subset size parameter k are not fixed in advance, and are considered user-defined parameters.

In subsection VI-A we introduce some classic datasets and visually compare DIPOLE with t-SNE or UMAP. In subsection VI-B we conduct a quantitative comparison for those same datasets, across a host of parameter values and quality measures, to get a more comprehensive picture of how DIPOLE compares with other, well-known methods. ⁴

A. Visualization Experiments

In this section, we apply DIPOLE to a number of datasets, and visually compare the results with other dimensionality-reduction methods. The datasets we consider are:

- A subsample of the mammoth data set from Smithsonian (2020). Cf. Figure 1.
- A point cloud sampled from a brain artery tree, taken from Bullitt et al. (2005) and analyzed in Bendich et al. (2016). Cf. Figure 2.
- A swiss roll data set of 3000 points with the interior of the cylinder $x^2 + (y - 1)^2 = 25$ subsequently removed. Cf. Figure 3.
- The *Stanford faces* dataset, consisting of 698 synthetic face images of 64×64 resolution, considered as a point cloud in \mathbb{R}^{4096} . The faces were captured as 2D images for a variety of pose and lighting parameters. Cf. Figure 4.

For each experiment, we compare the initial point cloud (or its Isomap visualization), DIPOLE, t-SNE or UMAP, and a degenerate version of DIPOLE where only the local metric regularizer is active (corresponding to $\alpha = 1.0$ in Equation (1)), denoted *local metric regularizer* (*lmr* for short). For the local metric regularizer experiments, we increase m_2 to 10 to improve its performance, giving local geometry a better chance of enforcing global structure. We see in many cases that local metric regularization alone does not suffice to produce an optimal embedding, and that the differences between its embedding and that obtained by DIPOLE are notably topological, in the relative configurations of distinct components or the appearance of important cycles.

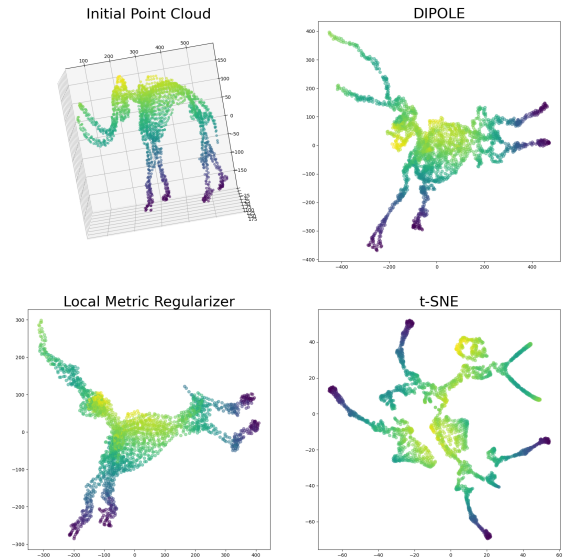


Fig. 1. Mammoth data set. Top Left: Initial point cloud. Top Right: DIPOLE with $m_1 = 5, m_2 = 3, \alpha = 0.1, k = 64, lr = 1.0$. Bottom Left: Setting $m_2 = 10$ and $\alpha = 1.0$, i.e. using only the local metric regularizer. Bottom Right: t-SNE default parameters.

⁴DIPOLE source code and scripts to run the experiments can be found at <https://github.com/aywagner/DIPOLE>

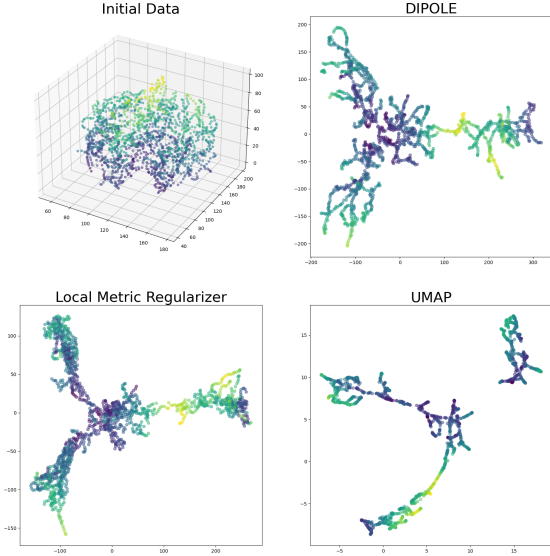


Fig. 2. Brain Artery Tree data set. Top Left: Initial point cloud. Top Right: DIPOLE with $m_1 = 5, m_2 = 3, \alpha = 0.1, k = 64, lr = 1.0$. Bottom Left: Setting $m_2 = 10$ and $\alpha = 1.0$, i.e. using only the local metric regularizer. Bottom Right: UMAP default parameters.

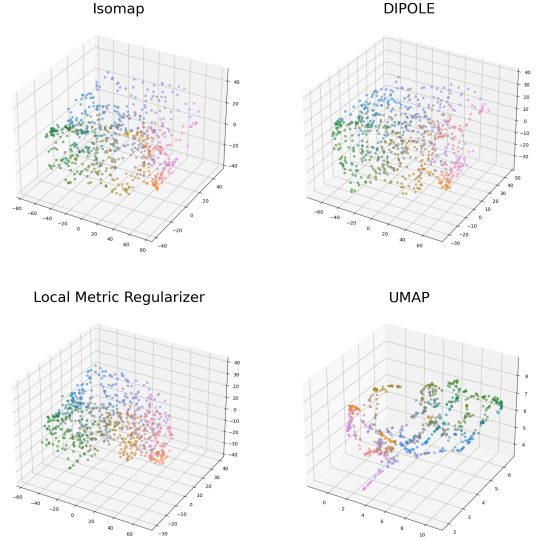


Fig. 4. Stanford Faces data set. Top Left: Isomap embedding. Top Right: DIPOLE with $m_1 = 5, m_2 = 5, \alpha = 0.1, k = 32, lr = 1.0$. Bottom Left: Setting $m_2 = 10$ and $\alpha = 1.0$, i.e. using only the local metric regularizer. Bottom Right: UMAP default parameters. The coloring scheme is RGB, with the pose parameter giving the red scale, and the lighting parameter the blue scale (green was fixed at 0.5).

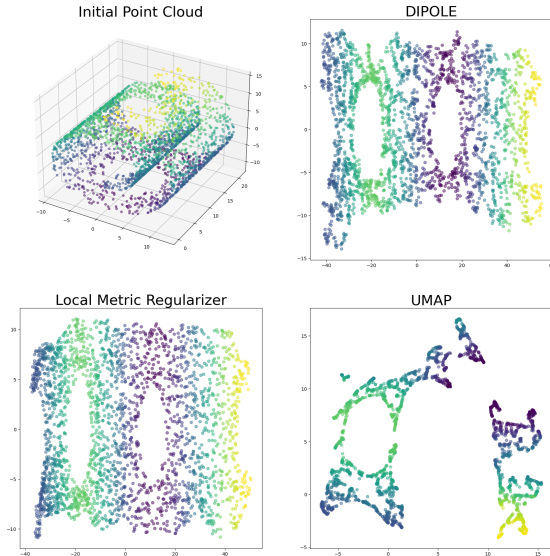


Fig. 3. Swiss Roll with Holes data set. Top Left: Initial point cloud. Top Right: DIPOLE with $m_1 = 10, m_2 = 3, \alpha = 0.1, k = 64, lr = 0.1$. Bottom Left: Setting $m_2 = 10$ and $\alpha = 1.0$, i.e. using only the local metric regularizer. Bottom Right: UMAP default parameters.

B. Quantitative Analysis

We now perform a quantitative comparison of DIPOLE with other dimensionality reduction methods. Quantitative comparison of different dimensionality reduction techniques is an active area of research without a standard test (Wang et al., 2020). The framework we adopt assumes that a dimensionality reduction method has access to three inputs: a point cloud $X \subseteq \mathbb{R}^D$, a target dimension $d < D$ in which to embed X , and a specification of an intrinsic metric on X , e.g. the geodesic metric on the graph whose edges correspond to the k nearest neighbors of each point in $(X, \|\cdot\|)$. We then compare dimensionality reduction techniques by their capacity to preserve this given intrinsic metric. That is, if (X, d_H) is the user-specified intrinsic metric on X , and (X, d_L) is the metric on X given by pulling back the Euclidean metric of its projection to \mathbb{R}^d , we are interested in measuring how well (X, d_L) maintained the structure of (X, d_H) according to various tests. It should be noted that all the tests are defined such that lower values represent superior performance.

The first test we consider is the ijk -test. This test measures the probability that the numerical order of $d_H(x_i, x_j), d_H(x_i, x_k)$ is preserved in d_L . Precisely, consider the random variable Z defined as follows. Randomly select x_i, x_j, x_k uniformly from the set X . If either $d_H(x_i, x_j) \leq d_H(x_i, x_k)$ and $d_L(x_i, x_j) \leq d_L(x_i, x_k)$ or $d_H(x_i, x_j) \geq$

$d_H(x_i, x_k)$ and $d_L(x_i, x_j) \geq d_L(x_i, x_k)$ then Z is 1; otherwise, Z is 0. The measure of interest is then $1 - E[Z]$, which we estimate empirically with 10000 samples.

The second test is the residual variance. Specifically, this is $1 - R^2$ where R is the Pearson correlation coefficient between the distance matrices corresponding to d_H and d_L , i.e. it is the cosine of the angle between d_H and d_L viewed as mean-centered vectors. This test was used in Tenenbaum et al. (2000) to quantitatively evaluate the success of Isomap.

The third and fourth tests are the 2-Wasserstein distance between approximations of the global persistence diagrams in degree 0 and 1 of d_H and d_L . Specifically, we perform farthest point sampling on d_H and d_L to obtain two subsets of size 256, compute the Rips persistence of the two metric subspaces, and finally report the 2-Wasserstein distance between the persistence diagrams.

The five dimensionality reduction techniques that we compare are Isomap, t-SNE, UMAP, DIPOLE, and DIPOLE with only the local metric regularizer. For each method, all combinations of the listed hyperparameters are computed. For DIPOLE, we initialize with Isomap and minimize the following

$$\frac{1 - \alpha}{2} \binom{|X|}{k}^{-1} \sum_{\substack{S \subset X \\ |S|=k}} \sum_{p=0}^1 W_2^2(D_p(S, d_H), D_p(S, d_L)) + \alpha \sum_{(i,j) \in P} (d_X(x_i, x_j) - \|a_i - a_j\|)^2, \quad (1)$$

where $D_p(S, d)$ is the degree p persistence diagram of the Rips complex of the metric space (S, d) .

For DIPOLE, the edges for the local metric regularizer are chosen to be either the 3 or 5 nearest neighbors in the Euclidean distance in \mathbb{R}^D . The subset size k is chosen to be either 32 or 64. The learning rate and α are chosen to be in $\{0.1, 1, 2\}$ and $\{0.01, 0.1\}$, respectively. We do not tune any hyperparameters for Isomap, using the default value of 5 for the number of nearest neighbors. For the local metric regularizer, we choose the number of edges in the neighborhood graph to be in $\{2, 3, 5, 10\}$ and the learning rate to be in $\{0.1, 1, 2\}$. For t-SNE, we choose 32 evenly spaced values between 2 and 75 for the perplexity hyperparameter. Finally, for UMAP, we choose the number of neighbors in $\{4, 8, 16, 32, 64, 128\}$ and the minimum distance parameter in $\{0, 0.1, 0.25, 0.5, 0.8\}$.

The results for the mammoth, brain, swiss roll with holes, and *Stanford faces* datasets are shown in Figure 5, 6, 7, and 8. Each figure has four panels corresponding to each of the four tests: ijk , residual variance, global degree 0 persistent homology, and global degree 1 persistent homology. In each panel, a histogram of scores is plotted for each method over all choices of hyperparameters. Since different methods use hyperparameter grids of different sizes, the histograms for some methods contain more points than the histograms for others; in particular, Isomap only has a single bar of height one in each figure because there was no hyperparameter tuning.

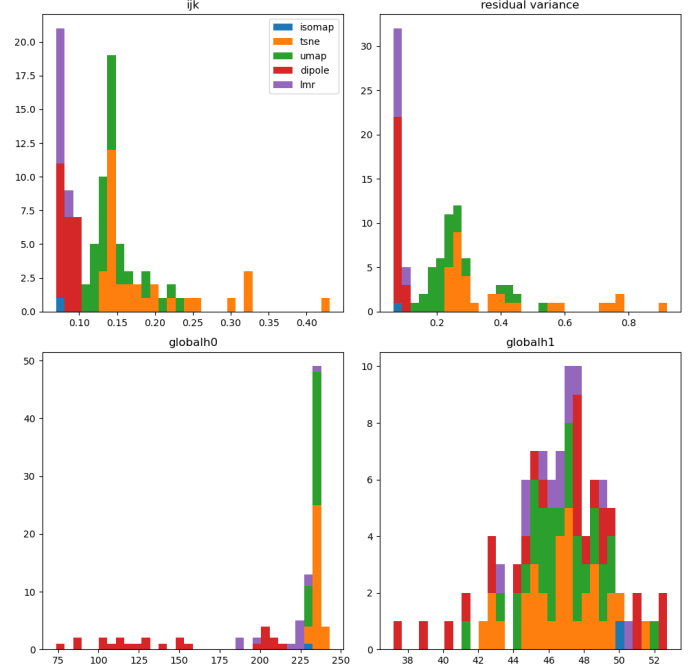


Fig. 5. Results for the mammoth dataset.

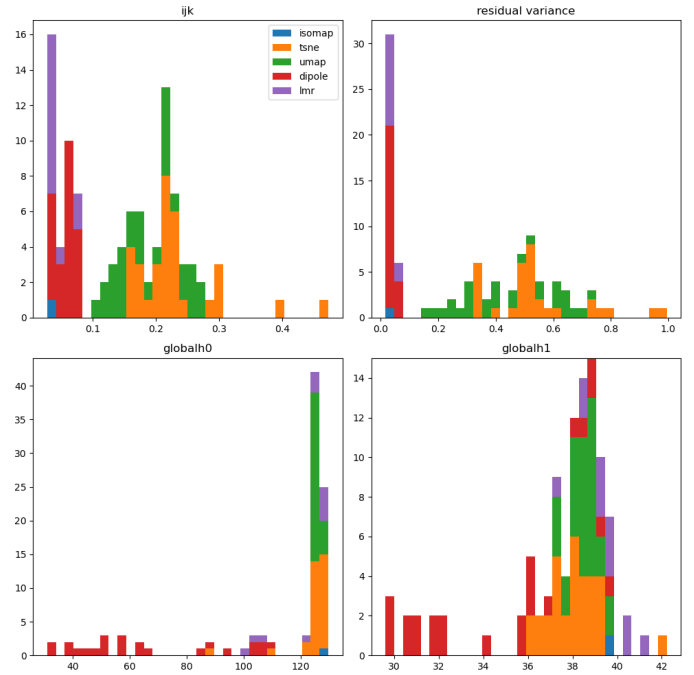


Fig. 6. Results for the brain dataset.

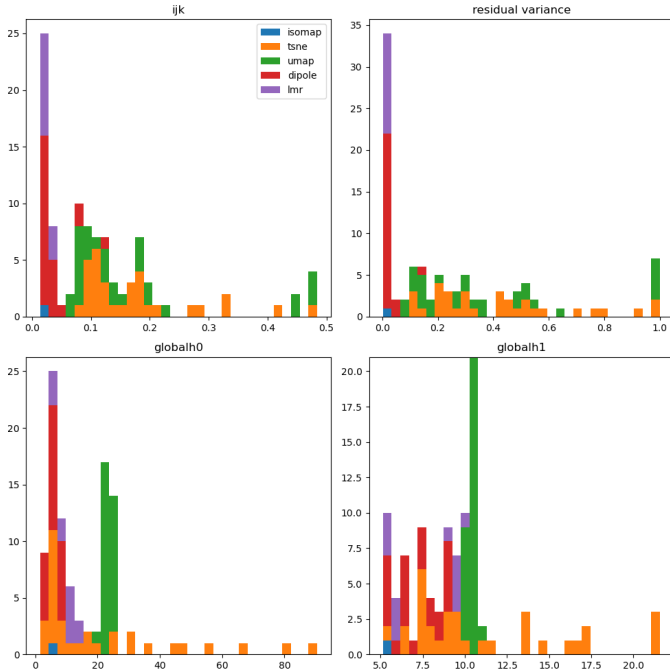


Fig. 7. Results for the swiss roll with a hole dataset.

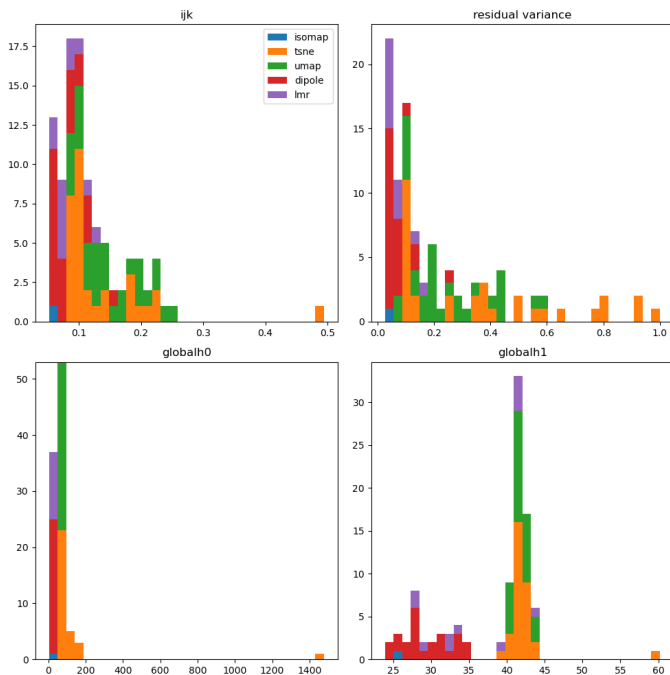


Fig. 8. Results for the *Stanford faces* dataset.

Dataset	Isomap	t-SNE	UMAP	DIPOLE	LMR
Mammoth	8.51	24.26	13.73	77.89	20.16
Brains	6.13	17.63	10.64	72.56	15.31
Swiss hole	9.70	28.04	16.31	81.60	23.47
Faces	6.73	15.80	8.64	75.61	16.80

Fig. 9. Average running time in seconds of each dimensionality reduction method and dataset over hyperparameter grid. Note that the computation of persistence diagrams of subsets is parallelizable and, though not implemented here, would result in a significant increase in the speed of DIPOLE.

In all the experiments, most of the hyperparameter choices for DIPOLE result in competitive embeddings with respect to the ijk and residual variance tests. Consistent with the images in Section VI-A, DIPOLE significantly outperforms all other methods in the degree 0 and 1 homology tests for the mammoth and brain datasets.

One limitation of our scheme for visualizing quantitative scores is that the distribution of scores for each test does not capture their full joint distribution, in that hyperparameters which perform well for one test might not perform well for another test. Readers interested in comparing quantitative scores at this level of granularity are invited to access the publicly available code, from which full tables of scores can be accessed.

Finally, in Figure 9, we give the average running time of each method and dataset over the hyperparameter grid. Two factors which contribute to the longer runtime of DIPOLE are the time spent computing an initial embedding, done in our experiments with Isomap, and the time spent computing persistence diagrams of size k subsets. In our code, persistence diagrams were computed sequentially, but computing multiple persistence diagrams in parallel, i.e. using a batch size larger than 1, would result in a substantial decrease in the runtime of DIPOLE. Indeed, this parallelizability was a motivating consideration in developing distributed persistence and will be a feature of future iterations of DIPOLE.

VII. CONCLUSION

Distributed persistence summarizes the multi-scale topology of a data set in a way that is scalable, robust, and differentiable. Combining distributed persistence with local metric information, **DIPOLE** forms a new approach to dimensionality reduction based on structured, topological invariants, and with strong theoretical guarantees.

The pipeline proposed in this paper is very flexible, and open to various modifications and improvements. These include different schemes for sampling subsets (e.g. random point neighborhoods for studying mesoscale phenomena in materials science), other topology-based metrics, alternative persistence constructions (e.g. witness complexes), etc.

Possible directions for future research include building a form of **DIPOLE** for shape registration and interpolation, as well as incorporating distributed persistent homology into machine learning pipelines for regression and classification.

REFERENCES

- Henry Adams, Tegan Emerson, Michael Kirby, Rachel Neville, Chris Peterson, Patrick Shipman, Sofya Chepushtanova, Eric Hanson, Francis Motta, and Lori Ziegelmeier. Persistence images: A stable vector representation of persistent homology. *Journal of Machine Learning Research*, 18, 2017.
- Mikhail Belkin and Partha Niyogi. Laplacian eigenmaps for dimensionality reduction and data representation. *Neural computation*, 15(6):1373–1396, 2003.
- Paul Bendich, James S Marron, Ezra Miller, Alex Pieloch, and Sean Skwerer. Persistent homology analysis of brain artery trees. *The annals of applied statistics*, 10(1):198, 2016.
- Peter Bubenik. Statistical topological data analysis using persistence landscapes. *J. Mach. Learn. Res.*, 16(1):77–102, 2015.
- Mickaël Buchet, Frédéric Chazal, Tamal K Dey, Fengtao Fan, Steve Y Oudot, and Yusu Wang. Topological analysis of scalar fields with outliers. *arXiv preprint arXiv:1412.1680*, 2014.
- Elizabeth Bullitt, Donglin Zeng, Guido Gerig, Stephen Aylward, Sarang Joshi, J. Keith Smith, Weili Lin, and Matthew G. Ewend. Vessel tortuosity and brain tumor malignancy: A blinded study1. *Academic Radiology*, 12(10):1232–1240, 2005. ISSN 1076-6332. doi: <https://doi.org/10.1016/j.acra.2005.05.027>. URL <https://www.sciencedirect.com/science/article/pii/S1076633205005647>.
- Mathieu Carriere, Frédéric Chazal, Marc Glisse, Yuichi Ike, and Hariprasad Kannan. Optimizing persistent homology based functions. 2021.
- David Cohen-Steiner, Herbert Edelsbrunner, and John Harer. Stability of persistence diagrams. *Discrete & computational geometry*, 37(1):103–120, 2007.
- Ronald R Coifman and Stéphane Lafon. Diffusion maps. *Applied and computational harmonic analysis*, 21(1):5–30, 2006.
- Justin Curry. The fiber of the persistence map for functions on the interval. *Journal of Applied and Computational Topology*, 2(3):301–321, 2018.
- Damek Davis, Dmitriy Drusvyatskiy, Sham Kakade, and Jason D Lee. Stochastic subgradient method converges on tame functions. *Foundations of computational mathematics*, 20(1):119–154, 2020.
- Vin De Silva and Joshua B Tenenbaum. Sparse multidimensional scaling using landmark points. Technical report, Technical report, Stanford University, 2004.
- Harish Doraiswamy, Julien Tierny, Paulo JS Silva, Luis Gustavo Nonato, and Claudio Silva. Topomap: A 0-dimensional homology preserving projection of high-dimensional data. *arXiv preprint arXiv:2009.01512*, 2020.
- Brittany Terese Fasy, Fabrizio Lecci, Alessandro Rinaldo, Larry Wasserman, Sivaraman Balakrishnan, Aarti Singh, et al. Confidence sets for persistence diagrams. *Annals of Statistics*, 42(6):2301–2339, 2014.
- Marcio Gameiro, Yasuaki Hiraoka, and Ipepei Obayashi. Continuation of point clouds via persistence diagrams. *Physica D: Nonlinear Phenomena*, 334:118–132, 2016.
- J. B. Kruskal. Multidimensional scaling by optimizing goodness of fit to a nonmetric hypothesis. *Psychometrika*, 29(1):1–27, 1964. doi: [10.1007/BF02289565](https://doi.org/10.1007/BF02289565). URL <https://doi.org/10.1007/BF02289565>.
- Leland McInnes, John Healy, and James Melville. Umap: Uniform manifold approximation and projection for dimension reduction. *arXiv preprint arXiv:1802.03426*, 2018.
- Yuriy Mileyko, Sayan Mukherjee, and John Harer. Probability measures on the space of persistence diagrams. *Inverse Problems*, 27(12):124007, 2011.
- Michael Moor, Max Horn, Bastian Rieck, and Karsten Borgwardt. Topological autoencoders. In *International Conference on Machine Learning*, pages 7045–7054. PMLR, 2020.
- Nina Otter, Mason A Porter, Ulrike Tillmann, Peter Grindrod, and Heather A Harrington. A roadmap for the computation of persistent homology. *EPJ Data Science*, 6:1–38, 2017.
- Adrien Poulenard, Primoz Skraba, and Maks Ovsjanikov. Topological function optimization for continuous shape matching. In *Computer Graphics Forum*, volume 37, pages 13–25. Wiley Online Library, 2018.
- Sam T. Roweis and Lawrence K. Saul. Nonlinear dimensionality reduction by locally linear embedding. *Science*, 290(5500):2323–2326, 2000. ISSN 0036-8075. doi: [10.1126/science.290.5500.2323](https://doi.org/10.1126/science.290.5500.2323). URL <https://science.sciencemag.org/content/290/5500/2323>.
- Albert D Shieh, Tatsunori B Hashimoto, and Edoardo M Airoidi. Tree preserving embedding. *Proceedings of the National Academy of Sciences*, 108(41):16916–16921, 2011.
- Smithsonian. Mammuthus primigenius (Blumbach), 2020. URL <https://3d.si.edu/object/3d/mammuthus-primigenius-blumbach:341c96cd-f967-4540-8ed1-d3fc56d31f12>.
- Elchanan Solomon, Alexander Wagner, and Paul Bendich. From Geometry to Topology: Inverse Theorems for Distributed Persistence. *arXiv e-prints*, art. arXiv:2101.12288, January 2021.
- Joshua B. Tenenbaum, Vin de Silva, and John C. Langford. A global geometric framework for nonlinear dimensionality reduction. *Science*, 290(5500):2319–2323, 2000. ISSN 0036-8075. doi: [10.1126/science.290.5500.2319](https://doi.org/10.1126/science.290.5500.2319). URL <https://science.sciencemag.org/content/290/5500/2319>.
- Laurens van der Maaten and Geoffrey Hinton. Visualizing data using t-sne. *Journal of Machine Learning Research*, 9(86):2579–2605, 2008. URL <http://jmlr.org/papers/v9/vandermaaten08a.html>.
- Yingfan Wang, Haiyang Huang, Cynthia Rudin, and Yaron Shaposhnik. Understanding how dimension reduction tools work: An empirical approach to deciphering t-sne, umap, trimap, and pacmap for data visualization, 2020.
- Lin Yan, Yaodong Zhao, Paul Rosen, Carlos Scheidegger, and Bei Wang. Homology-preserving dimensionality reduction via manifold landmarking and tearing. *arXiv preprint arXiv:1806.08460*, 2018.